Atmósfera 37, 401-424 (2023)
https://doi.org/10.20937/ATM.53167

Synoptic characteristics of the spatial variability of spring dust storms over Saudi Arabia

Khaled A. AL-ABBASI, Abdulhaleem H. LABBAN and Adel M. AWAD*

Department of Meteorology, King Abdulaziz University, P.O. Box 80208, Jeddah 21589, Saudi Arabia.
*Corresponding author; email: amawad@kau.edu.sa

Received: January 23, 2022; accepted: August 3, 2022

RESUMEN

El estudio estadístico y sinóptico de las tormentas de polvo de primavera sobre la Península Arábiga (PA) se estudió utilizando observaciones de 27 estaciones de superficie y datos meteorológicos del reanálisis de NCEP/NCAR para el periodo 1978-2008. El estudio muestra que espacialmente las regiones norte y este de la PA son las más afectadas por las tormentas de polvo y que, temporalmente, el periodo de estudio se puede dividir en dos subperíodos: antes y después de 1995, con un aumento pronunciado antes de 1995 y un aumento (disminución) suave después de 1995 con relación a los tipos de polvo (tormentas de polvo). El análisis sinóptico revela tres sistemas atmosféricos principales: sistemas frontales sobre la región norte, sistemas relacionados con la vaguada del Mar Rojo sobre la región occidental y sistemas térmicos bajos sobre la región oriental., Además, el estudio sinóptico muestra que todos los sistemas atmosféricos están asociados con un área de gradiente de presión (geopotencial) favorable, y que la forma y fuerza de los regímenes atmosféricos de viento máximo y capa superior son adecuados para integrar completamente las capas atmosféricas. Además, la baja térmica del sur es un componente sinóptico común de los sistemas atmosféricos relacionados con el polvo, pero su efecto es particularmente pronunciado en el sistema atmosférico de la región oriental.

ABSTRACT

Statistical and synoptic studies of spring dust storms over the Arabian Peninsula (AP) were performed using surface observations from 27 surface stations and meteorological data from the NCEP/NCAR reanalysis data set for the period 1978-2008. The study showed that, spatially, the northern and eastern AP are the regions most affected by dust storms and that, temporally, the study period can be divided into two subperiods: before and after 1995, with a pronounced increase before 1995 and a smooth increase (decrease) after 1995 with respect to dust (dust storms) types. The synoptic study reveals three main atmospheric systems: frontal systems over the northern region, Red Sea Trough (RST)-related systems over the western region, and thermal low systems over the eastern region. Additionally, the synoptic study shows that all the atmospheric systems are associated with a favorable pressure (geopotential) gradient area and that the shape and strength of the maximum wind and upper-layer atmospheric regimes are suitable for completely integrating the atmospheric layers. Moreover, the southern thermal low is a common synoptic component of dust-related atmospheric systems, but its effect is particularly pronounced in the atmospheric system of the eastern region.

Keywords: spring dust, synoptic system, Saudi Arabia, spatial dust variability.

1. Introduction

Mineral dust aerosols are one of the main factors affecting the Earth's climate system, air quality, biogeochemical cycles (Martin, 1991; Archer et al., 2000; Kok et al., 2018; Middleton, 2019), atmospheric chemistry (Dentener et al., 1996; Dickerson et

al., 1997; Martin et al., 2003), and ecosystem health (Prospero, 1999). Southwest Asia's arid deserts are among the nine main dust sources worldwide (Prospero et al., 2002; Goudie et al., 2021) and contribute approximately 20% of the total dust emissions globally (Tanaka and Chiba, 2006). The dust emission rate from these deserts is approximately equal to the dust emission rate from the Bodele depression and central Saharan dust sources in Africa (Hamidi et al., 2017). The Rub Al Khali desert along the Saudi Arabia-Oman border, shown in Figure 1a, has been identified as the most prolific dust source on the Arabian Peninsula (AP) according to the Total Ozone Mapping Spectrometer (TOMS) (Goudie and Middleton, 2001; Giles, 2005), the MODIS instrument (Butt et al., 2017; Ali et al., 2017), and ground-based measurements (Notaro et al., 2013; Prakash et al., 2015).

Studies of sources of dust in Southwest Asia have classified these sources into two main groups: local sources and remote sources (Notaro et al., 2013). Local sources include the Rub Al Khali, the Ad Dahna, the An Nafud, and the Syrian and Iraqi deserts, while remote sources include the Sahara (Washington et al., 2003; Osetinsky and Alpert, 2006; Hannachi et al., 2011; Awad and Mashat, 2014; Yu et al., 2013; Beegum et al., 2018; Mashat et al., 2021) (Fig. 1a). Specifically, among local sources, the alluvial plain of the Tigris and Euphrates Rivers in Iraq is recognized as the main dust source in the Middle East region (Sissakian et al., 2013; Zoljoodi et al., 2013; Namdari et al., 2018; Mohammadpour et al., 2021).

Using backward trajectories, Notaro et al. (2013) identified the Rub Al Khali desert as a major local dust source for western Saudi Arabia and the Sahara Desert as a major remote source (Mashat et al., 2021). For northern and eastern Saudi Arabia, the Syrian and Iraqi Deserts were identified as the primary dust sources.

Dust storms are prominent over Saudi Arabia during February-June, with a peak along the southern coast of the Red Sea occurring in mid-winter, a peak across northern Saudi Arabia around the An Nafud Desert occurring in spring, and a peak over eastern Saudi Arabia around the Ad Dahna Desert occurring in early summer (Notaro et al., 2013).

The main atmospheric dust systems influencing the Middle East region are frontal dust systems with strong winds associated with intense baroclinicity. These systems form in non-summer seasons because of the presence of high pressure over the southeastern

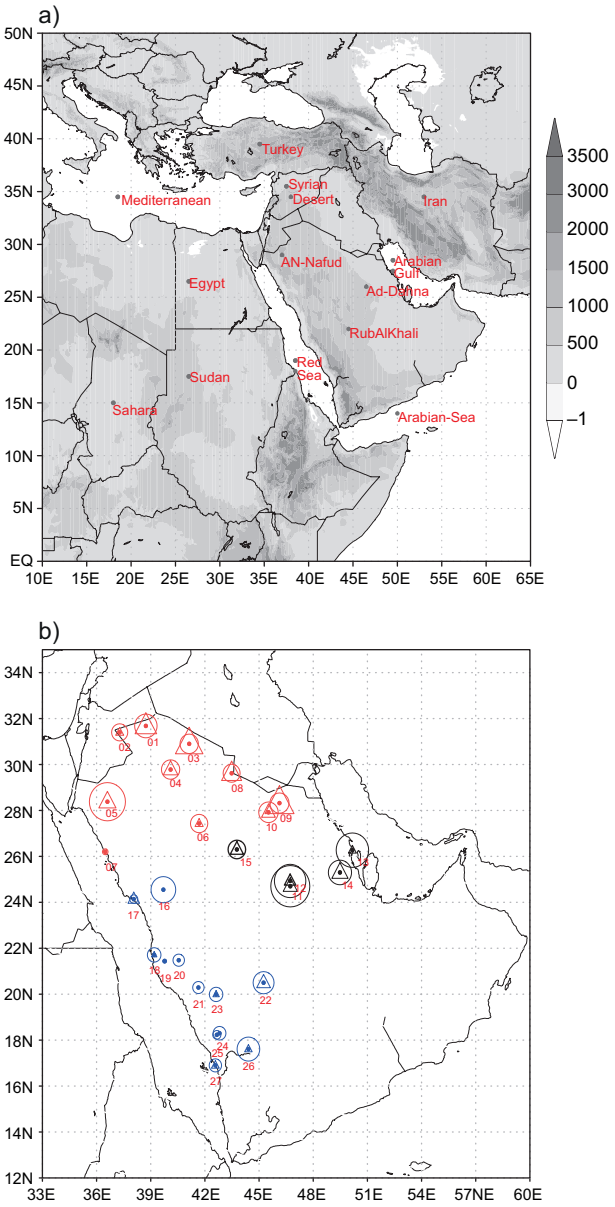

Fig. 1. (a) Topography of the study area and the main desert areas inside and near the AP. (b) The ratio of surface observed dust types (circles represent the dust and triangles represent the dust storm) at the surface stations within Saudi Arabia during spring. The size of the circles and triangles are proportional to the corresponding number of observed dust types that each surface station contributes with respect to the individual dust storm and dust types for 31 spring seasons

AP area and low pressure over the eastern Mediterranean region or due to the Siberian High over central Asia and low pressure over the eastern Mediterranean Sea (Middleton, 1986; Hermida et al., 2018; Francis et al., 2019; Hamidi, 2019; Mohammadpour et al., 2021, 2022). During February-April, the Mediterranean storm track is active, with passing cyclones and associated cold fronts carrying Saharan dust to Saudi Arabian stations along the northern coast of the Red Sea. Studies have shown that the most severe frontal dust storms occur during March and April (Hamidi, 2019) or they are generally prominent from February to June (Notaro et al., 2013; Yassin et al., 2018).

According to Abdi et al. (2011), dust storms are primarily triggered by dynamic lifting in the cool season in response to cold fronts and their associated mid-latitude troughs, or by diurnal vertical mixing in the warm season in response to solar heating. In turn, the radiative heating of dust aerosols can influence synoptic weather patterns (Islam and Almazroui et al., 2012; Liu et al., 2014; Zhao et al., 2015), e.g., increasing the Saudi Arabian heat low (Mohalfi et al., 1998; Francis et al., 2020).

Al-Jumaily and Ibrahim (2013) analyzed several dust storms in Iraq (northern AP) and found that their main driver is the passage of low-pressure systems over Iran, which carry cool air from the northern region toward a warmer region or warmer air over eastern Syria and Iraq (northern AP), following a temperature gradient (a front) formed or a releasing mechanism of dust formed along the Syrian Desert and over the eastern AP (Al-Dahna Desert) (Rao et al., 2001; Nabavi et al., 2017; Hamidi, 2019; Kaskaoutis et al., 2019; Hamzeh et al., 2021).

The concentration of atmospheric dust is tightly correlated with wind velocity (Kutiel and Furman, 2003; Kalenderski et al., 2013; Jish et al., 2015; Gandham et al., 2020). Strong surface cyclones can also stir up dust clouds or lift dust into the atmosphere along convergence zones, in monsoon regions, between cold air masses, and in association with cyclones and tropical anticyclonic air masses.

Atmospheric analysis of the synoptic patterns associated with or even favoring dust outbreaks over the AP is important for issuing forecasts and warning the public in cases of severe storms, and it could provide useful information about the atmospheric characteristics of dust events (Houssos et al., 2015; Hermida et al., 2018; Mashat et al., 2018).

Previous studies of dust systems influencing the AP (e.g., Goudi and Middleton, 2006; Hamidi et al., 2013; El Kenawy et al., 2014; Mashat et al., 2018; Rashki et al., 2019) did not differentiate between the atmospheric dust systems influencing different climate regions on the AP, but indicated that a combination of more than one of the atmospheric systems could influence dust systems. Therefore, the purpose of this study was to detect the specific atmospheric regimes influencing the individual regions of the AP (northern, western, and eastern regions) and to determine the spatial distribution of atmospheric dust systems.

This paper is organized as follows. In section 2 the data and methodology are described. Section 3 presents the statistical results of the surface measurements and the synoptic features of the different regions. The final two sections present the discussion and conclusions of the study.

2. Data and methodology

In this study, two sets of data were used: ground-based dust measurements from 27 surface stations in Saudi Arabia and 6-h meteorological reanalysis data from the National Centers for Environmental Prediction (NCEP/NCAR) from 1978 to 2008, with a horizontal spatial resolution of 2.5º × 2.5º (Kalnay et al., 1996; Kistler et al., 2001).

Daily surface observations of dust from 1978 to 2008 were retrieved from meteorological stations in Saudi Arabia (Fig. 1b). The surface station observations of dust and sand have been classified into two categories: the dust type, including suspended dust, and blowing dust, which have World Meteorological Organization (WMO) report codes (WW codes) 06 and 07, respectively; and the dust storm type, including dust storm observations with WW codes 09 and 30-32, and severe dust storm observations with WW codes 33-35 (WMO, 2005).

According to the WMO classification (WMO, 2005), Rashki et al. (2017), and Mashat et al. (2016), the characteristics of these types are as follows: (1) suspended dust (WW 06), widespread dust suspended in the atmosphere and not raised at or near the stations; (2) blowing dust (WW 07), dust or sand raised

at the time of observation; (3) dust storms (WW 09 and 30-32), large dust or sand quantities raised by strong winds with visibility < 1000 m but > 200 m; and (4) severe dust storms (WW 33-35), very strong wind lifting a large number of soil particles, with visibility < 200 m.

The synoptic evaluation of the composite maps for each region was performed based on the sea level pressure (SLP); the wind components at 850, 500, and 250 hPa; the vertical velocity at 850 hPa; the geopotential heights at 850 and 500 hPa; and the static stability in the 1000- to 500-hPa layer. The formula of the static stability used depends on Eq. (1):

$$-(T/\theta) \times (\partial\theta/\partial P) \quad (1)$$

where T is temperature and θ the potential temperature at pressure (P) levels of 1000 and 500 hPa (Gates, 1961).

To describe the spatial characteristics of the dust system, the AP can be divided into three dust regions based on previous dust studies (Middleton, 1986; Notaro et al., 2015; Awad and Mashat, 2016; Mashat et al., 2017, 2018, 2019) and not into five subregions as in Alobaidi et al. (2017) based on wet season climatological features. The northern region of dust (NRD) contains 10 stations (red stations in Fig. 1b), the western region of dust (WRD) contains 12 stations (blue stations in Fig. 1b), and the eastern region of dust (ERD) contains five stations (black stations in Fig. 1b), a list of detailed information for the stations used is in Table SI in the supplementary material.

This study statistically assessed the two observed dust types from two perspectives: spatially and temporally. In the first analysis, the spatial distribution of the two types at each station was represented by the frequency of each type. The size of the observation sample (circles for dust and triangles for dust storms; Fig. 1b) is proportional to the ratio of occurrences with respect to the relative observations at the other stations, i.e., the largest symbol size corresponds to the highest frequency, and the smallest symbol size corresponds to the lowest frequency. The temporal distributions, at annual and monthly scales, were calculated as the total number of observations over the entire area, i.e., as the number of observations per day from all stations.

In the synoptic study, to select the dust storm events associated with typical atmospheric systems in the entire AP and for each climate region, the following conditions were strictly followed:

1. Widespread dust events affected most of the AP, rather than only one or two climate regions, where these dust events affected at least one station in each of the three climate regions.
2. In each climate region, a dust event was defined in cases with at least one observation of a dust storm at the stations within the specific climate region but not observed at any station in other climate regions. For example, the cases in the northern region were those observed only at stations in the northern region and not observed at any of the stations belonging to the western or eastern regions.
3. For the case study, the second condition was used, but at least three stations had to have observed the dust storm.

This study defined the synoptic characteristics of AP dust events and the regional dust storm characteristics via the following steps:

a. Comparing the characteristics of composite events for different regions to determine how much the atmospheric dust characteristics differ among the different regions and to determine the specific characteristics that distinguish each region from the others.
b. Determining the common atmospheric characteristics associated with dust storm events influencing the AP.

3. Results

The spatial distribution of ground-based dust events (Fig. 1b) shows that most of the dust is concentrated in the northern and eastern regions at the Tabuk, Riyadh and Dhahran stations, in agreement with the surface observation results from Notaro et al. (2013), the aerosol optical depth (AOD) results from Ali et al. (2017), and the results from TOMS AI (Prospero et al., 2002; Washington et al., 2003). A moderate number of dust observations are present at the northeastern stations, i.e., Turaif, Arar, Hail,

and Hafrbaten, and at the western stations, especially Wadi-Aldawaser and Najran, which are close to the desert (Mashat et al., 2018). Additionally, the stations on the Red Sea or close to the Red Sea, such as Alwejh, Makkah, Yenbo, and Abha, have few dust observations (Notaro et al., 2013; Alobaidi et al., 2017).

Additionally, the spatial distribution of dust storm observations (Fig. 1b) shows that most of these are concentrated on the eastern boundary of the AP at the Turaif, Arar, Aljouf, Rafha, Alqaisumah, and Alhasa stations, as well as some other stations such as Tabuk, Hafrbaten, Riyadh(s), Gassim and Wadi-Aldawaser. In contrast, most stations close to the Red Sea, such as Alwejh, Makkah, Albaha, Almadinah, Jeddah, Altaif, Khamis-Mushait and Abha, have few observations of dust storms. Generally, the distribution of dust storms appeared similar to the annual distribution presented by Hermida et al. (2018) or the distribution of AOD (Ali et al., 2017).

The annual distribution of dust in Fig. 2a shows two distinct periods with different frequencies: from 1978 to 1994 and from 1995 to 2008. The first period has an annual average value of 1011.88 observations, corresponding to 37.48 observations per station. The annual average of observations in the second period is 1066, corresponding to 39.48 observations per station.

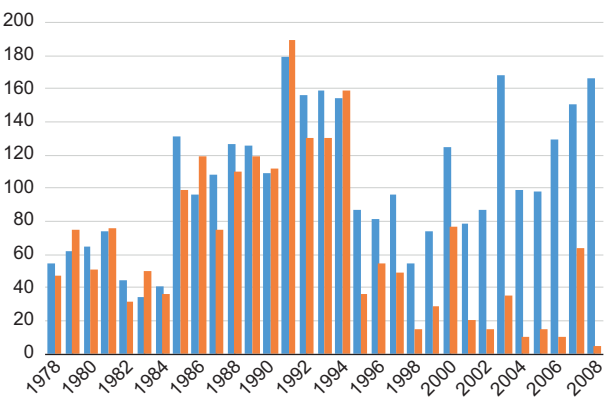

Fig. 2. (a) Annual distribution for the whole Saudi Arabia dust types (blue, each value multiplied by 10^{-1}), and (b) dust storm types (orange).

The annual distribution of dust storms in Fig. 2b shows three distinct periods. The first one, from 1978 to 1984, has an annual average of 52.43 observations or approximately two observations per station. The second period, from 1985 to 1994, has an annual average of 123.56 observations or approximately 4.6 observations per station. The third period, from 1995 to 2008, has an annual average of 31.14 observations or approximately 1.2 observations per station.

While the above results indicate that the period from 1985 to 1994 had a large number of dust phenomena, the period from 1978 to 1984 had the smallest number of dust phenomena observations. Furthermore, although the period from 1995 to 2005 had a large number of dust events, it had the smallest number of dust storm observations.

The monthly distribution (Table I) of dust shows that the average is approximately 326.4 350.1, and 359.8 observations/season in March, April, and May, respectively, indicating that the monthly average increases from cold months (March) to warm months (May), in agreement with the findings of Notaro et al. (2013) and Rezazadeh et al. (2013).

Table I. Monthly average observations of dust (types coded 5, 6, 7 and 8) and dust storms (types 9, and 30 to 35) for all stations.

Month	Dust	Dust storm
March	326.4	20.2
April	350.1	22.4
May	359.8	23.4

Generally, the annual distribution of spring months (Fig. 3) shows a wavy shape with a peak in the early 1990s and lows in the early 1980s and late 1990s.

In detail, although the monthly pattern is similar to the annual distribution of dust (Fig. 2a), the distribution has high variability in May (Fig. 3e) and low variability in March (Fig. 3a). In addition, the distribution indicated two trends: a rapidly increasing rate from 1978 to 1994 and a slowly decreasing rate from 1995 to 2004.

In March, from the annual distribution of dust storms (Fig. 3b), two periods of different trend rates were distinguished: an increasing rate period from 1978 to 1994, with an annual average of 30.18 cases or 1.1 cases for each station/season; and a low decreasing rate period from 1995 to 2008, with an

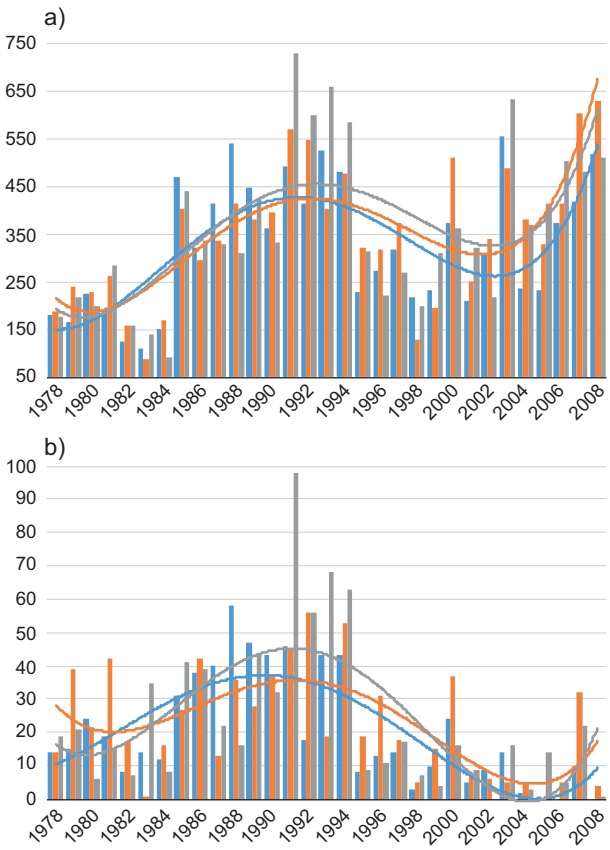

Fig. 3. Monthly distributions of (a) dust and (b) dust storm events (trends in curve shape) in March (blue), April (orange), and May (gray).

annual average of 8.1 cases or 0.3 cases for each station/season.

In April (Fig. 3d), two distinct periods were distinguished: the first from 1978 to 2000, with an annual average of 26.29 cases or 0.97 cases for each station; and the second from 2001 to 2008, with an annual average of 8 cases or 0.3 cases for each station.

In May (Fig. 3f), except for the four years from 1991 to 1994, which had a large number of cases with an annual average of 71.25 or 2.64 for each station, two periods were distinguished. The first one, from 1978 to 1990, had a low increasing rate, with an annual average of 23.46 cases or 0.87 cases for each station. The second period, from 1995 to 2008, had a very low decreasing rate, with an annual average of 9.57 cases or 0.33 cases for each station.

From the previous discussion, the monthly distribution appears similar to the first three clusters from Hermida et al. (2018), while the maximum number of dust cases was observed in May, not in March, as in Notaro et al. (2013).

3.1 Climate synoptic characteristics of widespread cases

In this subsection, the widespread cases (WSC), i.e., those cases influencing all three climate regions of the AP, were selected to represent the general dust storm events that affected the AP.

3.1.1 Mean sea level pressure and maximum wind at 250 hPa

Generally, widespread dust cases on the AP were influenced by two low-pressure centers (Fig. 4a): the northern center was located over Iraq and northeastern Saudi Arabia, with a lowest pressure value of 1006 hPa; and the southern center was located over the southwestern AP, with a lowest pressure value of 1005 hPa. Additionally, the previous low-pressure system was surrounded by either high-pressures or ridges, forming high-pressure gradient areas surrounding the AP.

The Azores high, with a high-pressure center of 1016 hPa over the southern Mediterranean and Libya locally known as Libyan high pressure (Washington and Todd 2005), formed a western pressure gradient area over the northwestern AP. The Arabian Sea high-pressure center, with a pressure value of 1010 hPa, interacted with the low-pressure system and formed the southern AP pressure gradient area. The ridge of the Siberian high, with a pressure value of 1008 hPa, over Iran and the Arabian Gulf (AG) (or Persian Gulf) interacted with the low-pressure system and formed the eastern pressure gradient area.

The maximum wind at 250 hPa (Fig. 4a), with a maximum value of 82 knots, has a trough shape over the northern Red Sea and an exit region over Iran. The maximum wind was observed to be a factor associated with dust storms over the region (Francis et al., 2019).

3.1.2 Geopotential height and vertical velocity at 850 hPa

At a pressure level of 850 hPa (Fig. 4b), the northern cyclone located over Turkey, with a value of 1450 gpm, exhibited a deep trough over the AP, and in conjunction with the subtropical anticyclone over Africa,

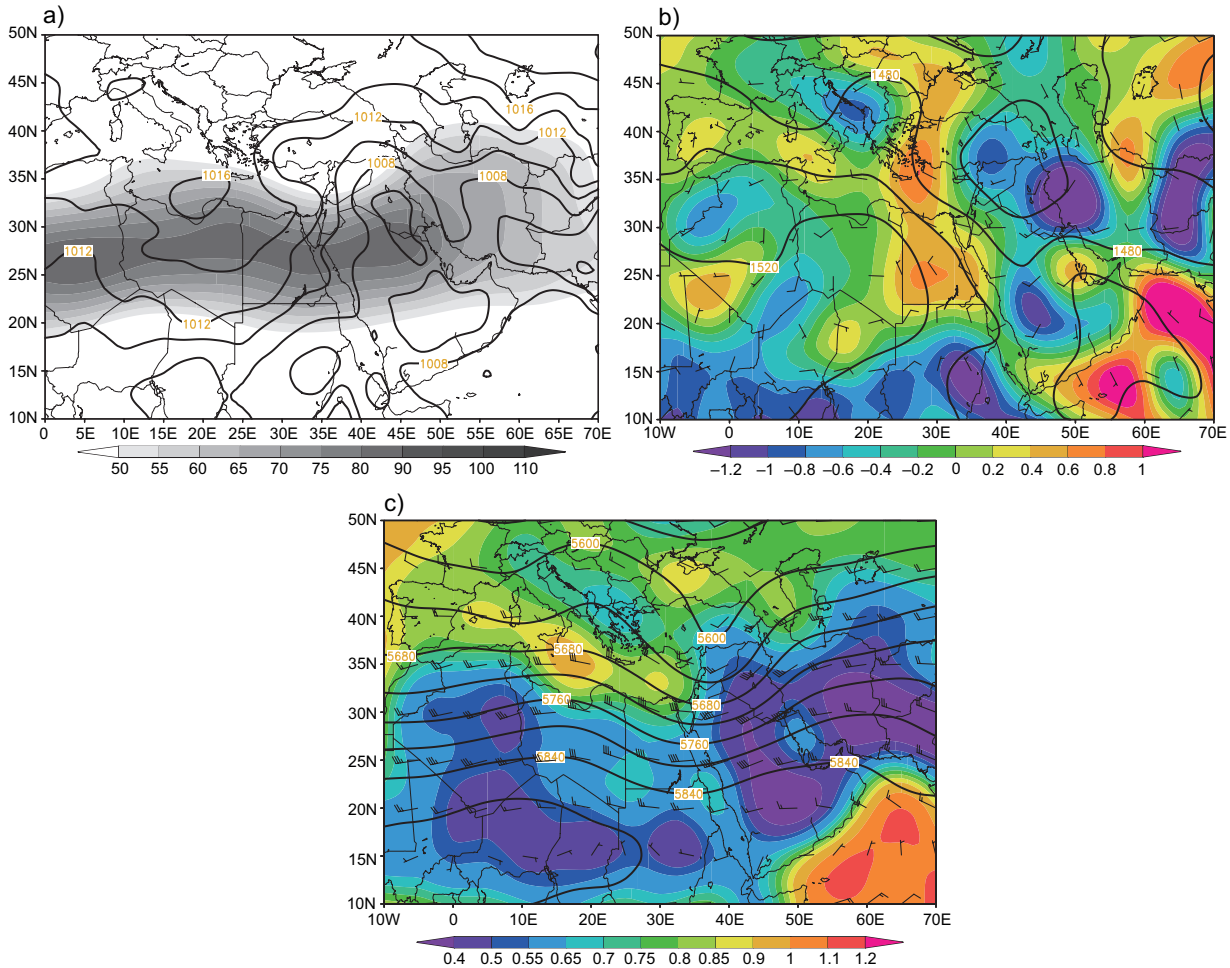

Fig. 4. Distributions of widespread composite for (a) mean sea level pressure (SLP) (isobars in hPa) and maximum wind speed at 250 hPa (shaded in knots); (b) geopotential height distributions, wind vectors and vertical velocities at the 850-hPa pressure level (contours in gpm, barbs in knots and shading in Pa s^{-1}, respectively), and (c) geopotential height distributions and wind vectors at the 500-hPa pressure level and static stability in the layer between 1000 hPa and 500 hPa (contours in gpm, barbs in knots and shading in deg db^{-1}, respectively) .

with a geopotential height of 1530 gpm, it formed an area of geopotential gradient over the western AP. The trough of the northern cyclone, in conjunction with the anticyclonic center with 1500 gpm over the Arabian Sea and southeastern AP, formed an area of geopotential gradient over the eastern AP and AG. The wind speed over the AP at this pressure level increased from south to north until reaching the northern AP, and then it decreased.

The distribution of omega at a pressure level of 850 hPa (Fig. 4b) shows that the vertical velocity followed the surface pressure systems, where upward motion accompanied low pressure, and downward motion accompanied the high-pressure centers or ridges. The highest upward motions (–1.0 and –1.2 Pa s^{-1}) were located over the southwestern AP and Iraq/Iran, respectively, while the highest downward motion (+1.0 Pa s^{-1}) was located over the Arabian Sea.

3.1.3 Geopotential height at 500 hPa and the static stability layer from 1000 to 500 hPa

At a pressure level of 500 hPa (Fig. 4c), the trough of the northern cyclone, with a geopotential value of 5560 gpm, extended southward over the Red Sea and eastern Africa, while the subtropical anticyclone over Africa, with a geopotential value of 5880 gpm,

formed a ridge over the eastern AP and AG. The wind speed at this level increased over the AP from south to north, ranging from 5 to 45 knots, and decreased, between 5 and 10 knots, from west to east.

The spatial distribution of the static stability (Fig. 4c) shows a low-stability area located over the AP, with a value of 0.4 deg db^{-1} and surrounded by high-stability areas. The high-stability areas surrounding the AP had values of 0.85, 1.1 and 0.85 deg db^{-1} over the Mediterranean Sea, the Arabian Sea and the northern region, respectively. Furthermore, two high-stability centers of 0.65 and 0.55 deg db^{-1} were formed over the Red Sea and AG, respectively. The interaction between the low stability area over the AP and the surrounding high-stability areas formed areas of a stability gradient around the AP, with a weak gradient area over the eastern AP.

3.2 Climate synoptic characteristics of the classified regions

In the following sub-section it can be seen that for each climate region the composite of the dust event satisfied the identifying conditions for the climate regions.

3.2.1 Mean sea level pressure and maximum wind at 250 hPa

Analysis of the atmospheric systems associated with the dust cases influencing the NRD (Fig. 5a) shows that this region was influenced by a low-pressure system, with a value of 1008 hPa and a deep trough over the AP, i.e., 2 hPa lower and located north of the corresponding system in WSC. The Azores high is associated with a high-pressure center with a value of 1017 hPa over northern Libya (Libyan high pressure), i.e., 1 hPa higher than the corresponding system in WSC, and a ridge over the eastern Mediterranean region. The Siberian high, with a value of 1019 hPa, is associated with a ridge over the AG. The Sudan low, with a value of 1005 hPa, is associated with the RST over the western Red Sea and extends northward to southern Egypt, i.e., extending northward farther than the WSC. The southern AP low pressure, with a value of 1007 hPa (less deep than the WSC), has two troughs, a weak one over the western AP and a strong one over the eastern AP, and is linked with the northern low-pressure system with a value of 1008 hPa, i.e., 2 hPa higher than the corresponding system

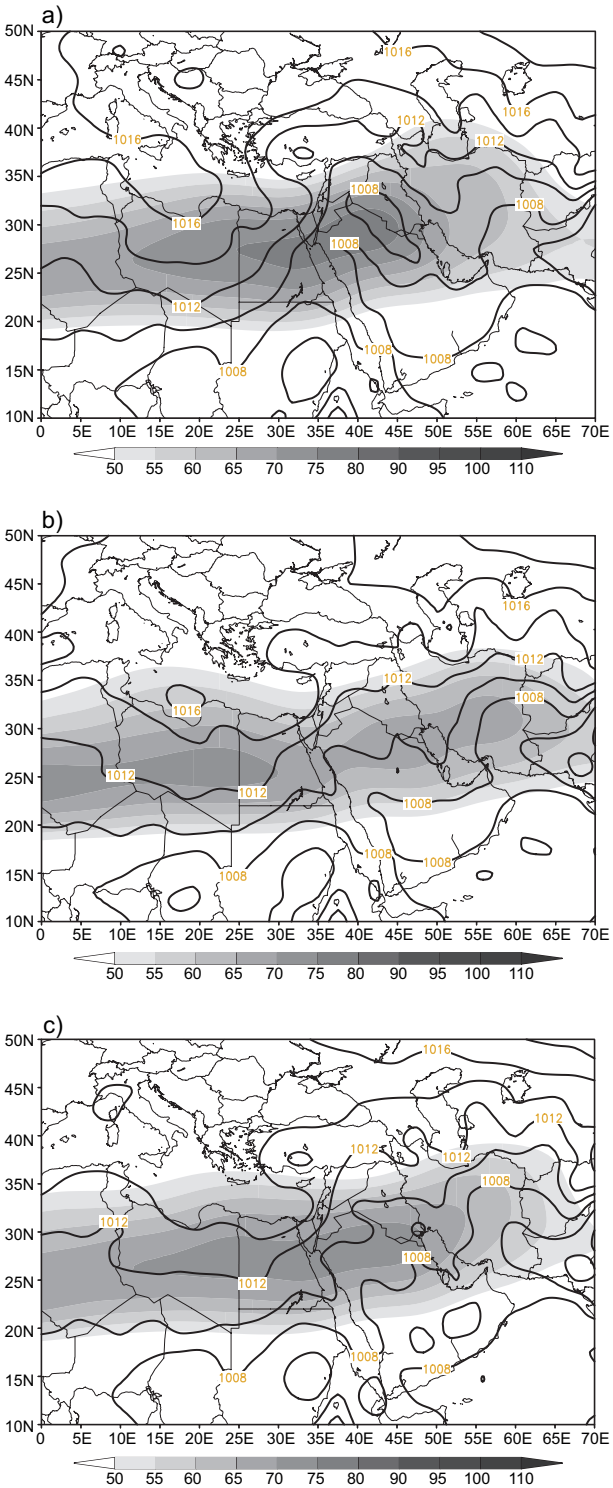

Fig. 5. Distributions of mean sea level pressure (SLP) (isobars, in hPa) and maximum wind speed at 250 hPa (shaded, in knots) for seasonal composites of the (a) northern (b) western, and (c) eastern regions.

in the WSC. This atmospheric regime is known as the frontal dust system (Hamidi et al., 2013).

The southern low-pressure system forms a strong pressure gradient area over the eastern Mediterranean region with the Azores ridge, and the north-south low-pressure system forms a pressure gradient with the Siberian ridge over Iraq and western Iran. These pressure gradients have been considered a characteristic of dust events because they increase the wind speed over a large area (Zoljoodi et al., 2013; Al-Yahyai and Charabi, 2014; Hermida et al., 2018).

The maximum wind at 250 hPa (Fig. 5a) shows that the core with the highest wind speed is located over the northern AP, with a value of 77 knots, i.e., 5 knots less than that of the WSC, and it forms a trough-shaped structure over the eastern Mediterranean region.

Analysis of the atmospheric systems influencing the WRD (Fig. 5b) shows that the Azores high is associated with a high-pressure center, with a value of 1016 hPa over Libya and a ridge over the eastern Mediterranean region. The Siberian high, with a value of 1019 hPa, has a pronounced ridge over the AG; i.e., its ridgeline is located eastward of that of the WSC. The Sudan low, with a value of 1005 hPa, is associated with a pronounced RST over the western Red Sea and extends northward to southern Egypt, i.e., extending farther northward than that of the WSC. The southern AP low pressure, with a value of 1007 hPa, has a pronounced trough over the western AP, i.e., deeper than that of the WSC, and it forms a gradient area with the Azores ridge over the eastern Red Sea, northern AP and Levant. Both the Siberian and Azores ridges form a wave-shaped pressure gradient area with a southern AP low-pressure system over the northern AP.

The core of the maximum wind of 250 hPa (as shown in Fig. 5b), is located over the eastern AP and northern AG and appears south of the composite results for the NRD. Additionally, an elongated core with a value of 72 knots, i.e., 5 knots slower than that of the WSC, extends over the Saharan region to central Egypt. The maximum wind forms a pronounced trough-shaped structure over the eastern Mediterranean and Red seas.

In the analysis of dust in the ERD (Fig. 5c), the Azores high is associated with a high-pressure center over southern Italy, with a value of 1016 hPa, and a pronounced ridge over the eastern Mediterranean and Red seas. The Siberian high, with a value of 1018 hPa, is associated with a ridge over the AG. The Sudan low, with a value of 1005 hPa, is associated with an RST over the western Red Sea, and the southern AP low pressure, with a value of 1006 hPa (i.e., less deep than the WSC by 1 hPa), has two cores over the southwestern and southeastern AP (rather than only one core, as in the WSC), representing one of the main dust systems that influence the region (Hamidi et al., 2014). Additionally, the southern low pressure has two troughs over the eastern and western AP and, with the Siberian and Azores systems, forms a pronounced wave-shaped pressure gradient over the AP, which, as noted by Hamidi et al. (2013), might transport dust from the Tigris and Euphrates area.

The maximum wind at 250 hPa (Fig. 5c) has a core over the northern AP with a value of 72 knots, and it is located to the south of its locations in the previously discussed situations. This southward shift of the maximum wind was explained by Perrone (1981) and Francis et al. (2019) as the southward progression of the polar jet in the AP, which enhanced the shamal wind. The maximum wind forms a trough shape over the eastern AP. The atmospheric systems associated with the dust events of this region are similar to clusters 1 and 2 (Hermida et al., 2018), and the relevant results suggest that the remote source of dust in these systems is the Syrian and Iraqi deserts, while the main source is the Rub'al Khali Desert.

3.2.2 Geopotential height and vertical velocity at 850 hPa

Analysis of the atmospheric systems affecting the dust conditions in the NRD (Fig. 6a) shows that the northern cyclone, defined by the 1460 gpm contour, has a pronounced trough over the northern AP, in agreement with the April cases (Beegum et al., 2018). Obviously, the NRD northern cyclone is less deep; its trough weakens southward and appears to the west of the corresponding trough in the WSC. The subtropical anticyclone has two branches. One branch is located over Africa and has a value of 1530 gpm and a ridge extending eastward to the western AP. The other branch is located over the AP and has a value of 1510 gpm and a ridge extending over the

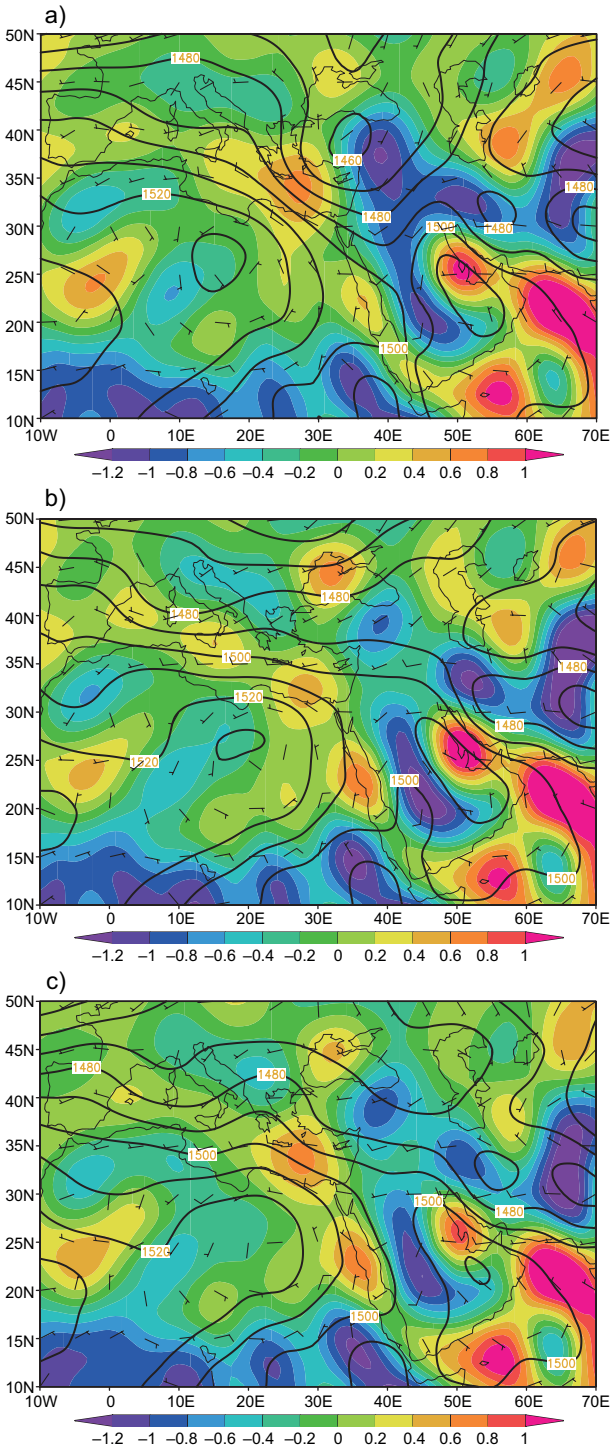

Fig. 6. Geopotential height distributions, wind vectors, and vertical velocities at the 850-hPa pressure level (contours in gpm, barbs in knots and shading in Pa s^{-1}, respectively) for regional composites of the (a) northern (b) western, and (c) eastern regions.

northern AP to Iraq, i.e., farther north than that of the WSC. The cyclonic and anticyclonic systems form two areas with geopotential gradients: one over the eastern Mediterranean and one over the northern AP and AG. The distribution of wind values shows that the wind decreases from west to east and from south to north.

The vertical velocity (Fig. 6a) forms a series of areas with upward and downward motions around the AP, including downward motion over the Red Sea, upward motion over the western AP and Levant, and downward motion over the AG. The highest values of downward motion are 0.4 and 1.0 Pa s^{-1} over the Red Sea and AG, respectively. The highest values of upward motion are –1.0 and –1.2 Pa s^{-1} over the southern AP and Levant, respectively.

The composite of the dust cases in the WRD (Fig. 6b) shows that the African branch of the subtropical anticyclone, with a value of 1530 gpm, shrank westward to eastern Africa and that the AP branch, with a value of 1510 gpm, shrank toward the eastern AP. The northern cyclone trough, with a value of 1490 gpm, flattened over the northern AP, while the tropical cyclone trough extended northward to the central AP. Obviously, the WRD northern cyclone weakened with depth, while the tropical cyclone deepened in comparison with the corresponding system in the WSC. The wind in this situation increased from west to east but was weaker than that in the NRD. The high wind in the NRD could be explained by frontal systems (Hamidi, 2019)

Although the general features of vertical velocity (Fig. 6b) are similar to those for the dust composite of the NRD, the magnitude of the vertical velocity changed to –1.2 and –0.8 Pa s^{-1} over the AP and Levant, respectively. The downward motion became 0.6 and 1.0 Pa s^{-1} over the Red Sea and AG, respectively. These changes show that the vertical velocity in the dust composite for the WRD intensified over the western regions, the Red Sea, and the western AP and AG, while it decreased over the Levant.

The composite of the dust cases influencing the ERD (Fig. 6c) shows that a subtropical anticyclone over Africa, with a value of 1530 gpm, extends eastward to the western AP, i.e., it is 30 gpm higher than the corresponding system in the WSC. A subtropical anticyclonic center, with a value of 1510 gpm, covers the eastern part of the AP. A tropical cyclone, with a value of 1490 gpm, is located over the tropical region

southwest of the Red Sea. A northern cyclone, with a value of 1470 gpm, has a weak trough over the Levant, i.e., less deep than that in the WSC. In addition, a pronounced cyclonic center over Iran, with a value of 1470 gpm, forms an area of geopotential gradient over the AG and western Iran with the Arabian anticyclonic center. The wind speed in this composite decreases from west to east.

In this composite (Fig. 6c), the features of the vertical velocity are similar to those in the other composites, but the magnitude and area of vertical velocity are different. The downward motion over the Red Sea, with a value of 0.6 Pa s^{-1}, extends slightly eastward over the AP. The downward motion over the AG, with a value of 0.8 Pa s^{-1}, is smaller. The upward motion over the AP has a value of 1.0 Pa s^{-1} and is slightly larger in response to similar mechanisms discussed previously.

3.2.3 Geopotential height at 500 hPa and the static stability layer from 1000 to 500 hPa

The northern cyclone in the NRD composite (details in Fig. S1a in the supplementary material), has a trough over the eastern Mediterranean and Egypt, i.e., to the west of that in the WSC. Additionally, a belt of low stability is observed over the Sahara, the AP and Iran, surrounded to the north and south by belts of high stability.

In the WRD (Fig. S1b) the trough of the northern cyclone is oriented more eastward and appears relatively flatter than those in the NRD and WSC. Additionally, the areas of low stability over the northern and southern AP shrank and expanded, respectively.

Based on the composite of dust events in the ERD (Fig. S1c), the trough of the northern cyclone shifted eastward compared with that in the above composites. Additionally, a new weak trough appeared over the eastern AP. The stability distribution of the ERD is similar to that in the composite for the other regions but increased over the Red Sea and decreased over the AG.

3.3 Case study

For each case study of the climate regions, the composite of the dust events was defined for dust cases for which at least three stations observed dust storm events within the specific climate region, but there were no dust storm events observed at any station in other climate regions.

3.3.1 Mean sea level pressure and maximum wind at 250 hPa

The synoptic features of the NRD cases (Fig. 7a) show that the northern cyclone over the Levant, with a value of 1006 hPa, is associated with a northwest-southeast trough over the northeastern AP. The southern cyclone, with a value of 1007 hPa, is associated with a weak trough over the southwestern AP. The Sudan low, with a value of 1005 hPa, is associated with an RST extending northward into southern Egypt. The Azores high is associated with a high-pressure center over northern Libya, which has a value of 1018 hPa and a ridge over the eastern Mediterranean region. The Siberian high, with a value of 1019 hPa, is associated with a ridge over western Iran. In conjunction with the northern cyclone over the Levant, these high-pressure or ridge systems form two areas with high-pressure gradients over the eastern Mediterranean and over Iraq. The maximum wind (Fig. 7a), with a value of 84 knots, i.e., greater than WSC by 2 knots, forms a trough shape over the northern AP.

In the WRD cases (Fig. 7b), the high-pressure center over Libya, with a value of 1016 hPa, extends over northern Libya and Egypt, and a southwest-northeast oriented ridge extends over the eastern Mediterranean. Additionally, the high pressure center forms a pronounced ridge over the Red Sea, reaching south to approximately 18º N. The Siberian high is associated with a high pressure center, with a value of 1011 hPa, over the northern AG region. The southern cyclone, with a value of 1007 hPa, has a pronounced trough over the western AP. The Sudan low, with a value of 1005 hPa, is associated with an RST extending northward to northern Sudan. With the trough of southern low pressure, the high-pressure ridge over the Red Sea and the high-pressure center over northern AG form two areas with pressure gradients over the western AP and the central AP. The maximum wind (Fig. 7b) has a core with a value of 77 knots over the northern AP, i.e., 5 knots less than the WSC, and it forms a weak trough shape over the northern Red Sea.

The atmospheric systems that characterize the ERD cases (Fig. 7c) show that the high-pressure center over the eastern Mediterranean, with a value of 1015 hPa, is associated with a weak pressure gradient over the eastern Mediterranean and a pronounced ridge over the Red Sea, extending southward to

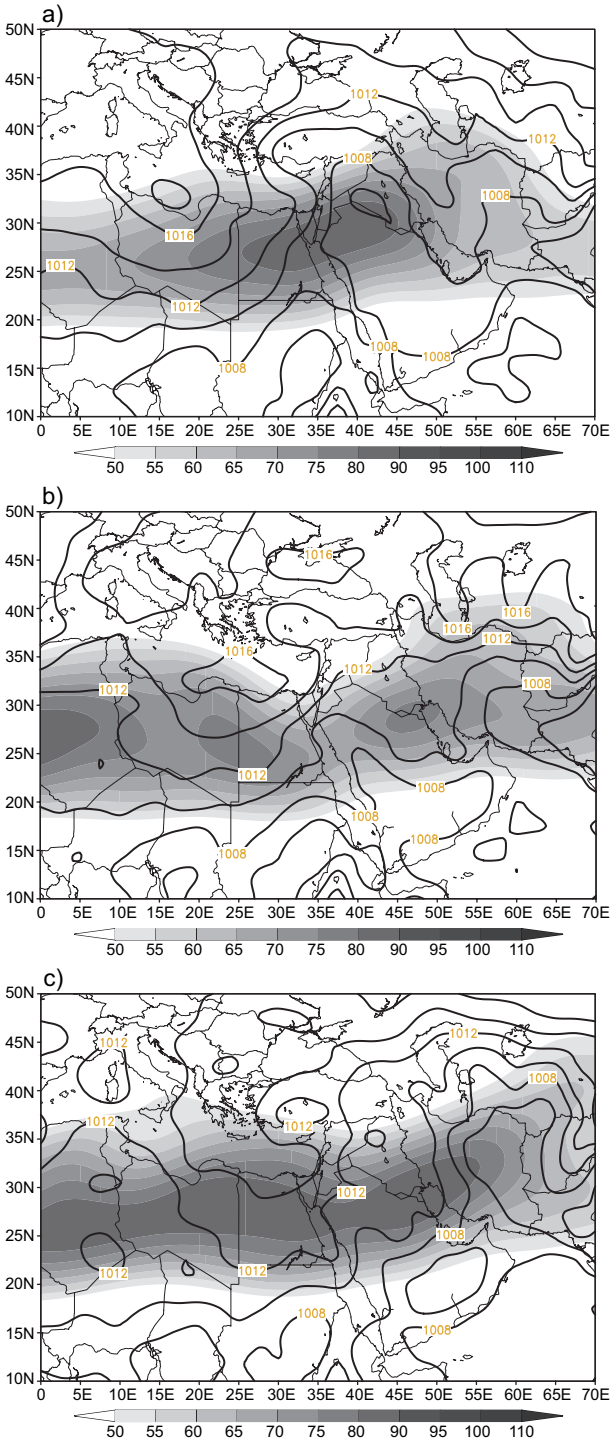

Fig. 7. Distributions of mean sea level pressure (SLP) (isobars in hPa) and maximum wind speed at 250 hPa (shaded in knots) for seasonal composites of the (a) northern (b) western, and (c) eastern regions.

approximately 17° N. The Siberian high, with a value of 1017 hPa, has a weak, flat ridge over the eastern AP. In contrast, the Sudan low, with a value of 1007 hPa, has a wide trough over Sudan. The southern low pressure, with a value of 1005 hPa, has a core over the southeastern AP and forms two troughs over the AP. A weak trough is located over the eastern region, and a relatively strong trough is located over the western region, although the eastern trough has a relatively high-pressure gradient area extending north-south over the eastern AP. The maximum wind (Fig. 7c) has a core with a value of 85 knots that extends over northern Africa and the northern AP, i.e., greater than WSC by 2 knots, and it forms a trough shape over the AP.

3.3.2 Geopotential height and vertical velocity at 850 hPa

In the NRD cases (Fig. 8a), the northern cyclone, with a value of 1440 gpm, has a pronounced trough over the northern AP. The tropical cyclone, with a value of 1490 gpm, has a trough over Sudan. The subtropical anticyclone over Africa, with a value of 1530 gpm, has a ridge extending eastward to the eastern Red Sea. The subtropical anticyclone center over the eastern AP, with a value of 1510 gpm, appears to relate to the African anticyclone and forms an anticyclonic, bell-shaped structure over the southern region. The above systems interacted with each other, and the northern cyclone trough formed a distinct shape over the eastern Mediterranean, Levant and northern AP. The wind over the AP decreased from west to east and from north to south. Additionally, a pronounced anticyclone wind pattern formed over the eastern AP.

The vertical velocity in the NRD cases (Fig. 8a) shows a series of downward and upward motions from west to east of the AP. The downward motion over eastern Africa and the Red Sea are extensions of downward-motion cores over the Mediterranean and Arabian Sea, with values of 0.6 and 1.0 Pa s^{-1}, respectively. Most of the AP, from the west, influenced the upward motion with a value of –1.0 Pa s^{-1}, while the northern AP and Levant have a high upward motion of –1.2 Pa s^{-1}. In contrast, the AG has a high downward motion of 1.0 Pa s^{-1}. This distribution of vertical velocity forms a high-gradient vertical velocity area over the AP, with a relatively large scale over the Levant and northern AP.

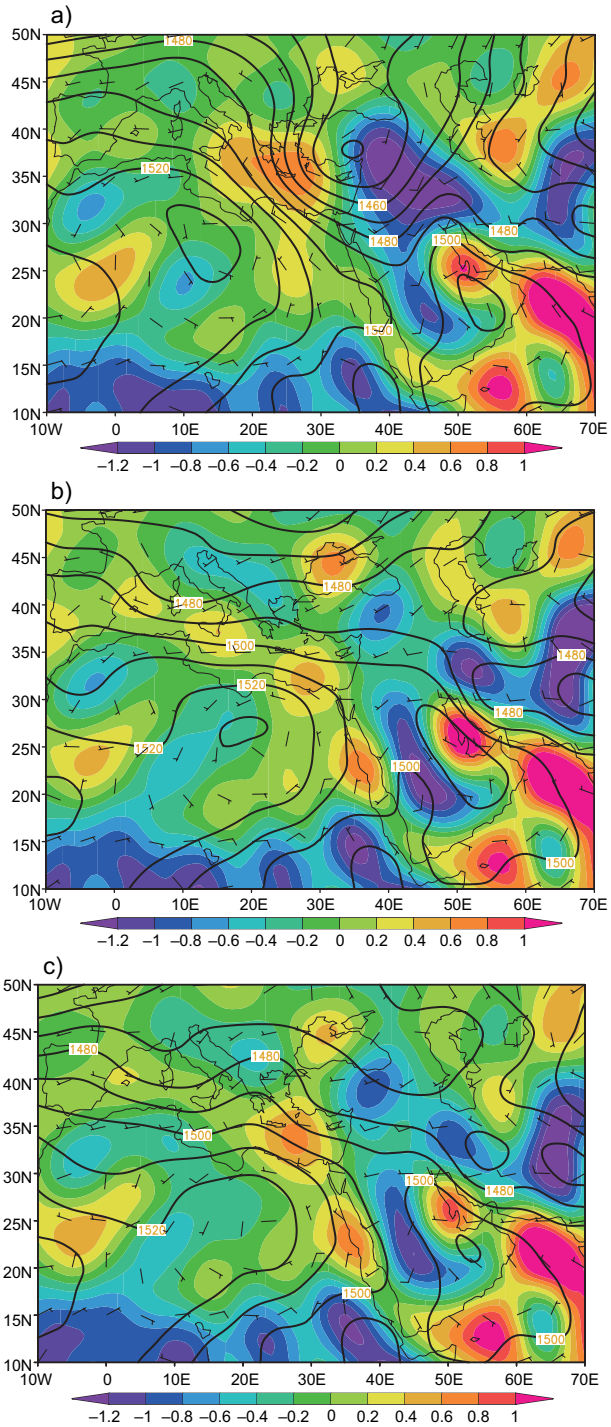

Fig. 8. Geopotential height distributions, wind vectors, and vertical velocities at the 850-hPa pressure level (contours in gpm, barbs in knots and shading in Pa s^{-1}, respectively) for regional composites of the (a) northern (b) western, and (c) eastern regions.

In the WRD cases (Fig. 8b), the African anticyclone shrank westward, and the AP anticyclone shrank until it was over the eastern AP. The northern cyclone trough shrank northward and became flat. The tropical cyclone extended northward over the entire western AP. The wind over the AP decreased from south to north over the western AP, and a pronounced anticyclone wind pattern formed over the eastern AP. Also, the core of high vertical velocity shifted southward over the central Red Sea, where it exhibited a downward-motion value of 0.8 Pa s^{-1} and undertook an upward motion over the western AP, where it exhibited a value of –1.2 Pa s^{-1}. The downward motion over the AG expanded. This distribution formed a high-gradient area of vertical velocity over the AP, especially over the western AP.

In the ERD cases (Fig. 8c), the African anticyclone, with a value of 1530 gpm, extended eastward over the western AP. A new core of the northern cyclone, with a value of 1440 gpm, located over the Caspian Sea formed two troughs: a weak trough over the northern AP and a strong trough over Iran. The tropical cyclone, with a value of 1490 gpm, extended northward over the central AP to the east of the WRD. These systems formed an area of geopotential gradient over AG and Iran and became stronger northwestward over the eastern AP. It is also observed that the core of the maximum upward motion shifted southward, with a value of -1.1 Pa s^{-1} over the AP, and a high-value area, with a value of -1.1 Pa s^{-1}, was also observed over Turkey. In addition, the values of downward motion over the Red Sea and AG were 1.0 Pa s^{-1} and 0.8 Pa s^{-1}, respectively. Therefore, the downward motion increased over the Red Sea and decreased over the AG.

3.3.3 Geopotential height at 500 hPa and the static stability layer at 1000-500 hPa

The northern cyclone associated with the NRD cases (see details in suppl Fig. S2a) has a deep trough over the eastern Mediterranean and eastern Africa. The subtropical anticyclone has pronounced ridges over western Africa and the AP. Additionally, the stability distribution shows a low stability over the AP, Iran and Pakistan. The low-stability areas over the AP interacted with the surrounding high-stability areas forms areas with stability gradients around the AP.

For the WRD cases (Fig. S2b), in comparison with that of the NRD cases, the trough of the northern cyclone is shifted eastward, while the subtropical anticyclone is shifted eastward and is relatively flatter. Additionally, the African stability decreased, and the stability generated two new centers of low stability over the northern and southern AP.

For the ERD cases (Fig. S2c), in comparison with that of the WRD cases, the trough of the northern cyclone is shifted eastward. The Arabian ridge is flat, while the African ridge becomes pronounced. Additionally, the low-stability area over the AP is shifted to the southern region and the high-stability areas extend over the Mediterranean and the Red Sea.

4. Discussion

The results of this study were based on a statistical study of surface observations of dust and dust storm types for selected cases affecting individual regions, which influenced more than two regions, and on meteorological data from the NCEP/NCAR reanalysis data set to determine the synoptic characteristics of the regional composites and widespread composite.

The spatial distributions of dust and dust storms demonstrated that most of the area north of 24º N is strongly affected by dust phenomena, in agreement with the findings of Kutiel and Furman (2003). Additionally, the Dawasir station, which is close to the desert, is also strongly affected (Notaro et al., 2013).

The spring monthly average of dust (dust storm) events indicated that the dust (dust storm) event frequency increased with warming from month to month, in agreement with the findings of Notaro (2015). The annual distribution of dust (dust storms) showed a wavy shape, with a high, increasing rate in the first study period until 1994 and a low, increasing (decreasing) rate in the second study period until 2004.

Although the monthly annual distribution of dust (dust storms) stations could be divided into two periods with different rates, the distribution in March exhibited pronounced changes, while the distributions in April and May exhibited small changes.

The synoptic climatology of the different regions indicated that the pronounced atmospheric systems in the NRD are the northern low-pressure system and its connection with the southern low-pressure system over the AP. In addition, the different atmospheric systems that interacted and produced areas of pressure gradient around the northern AP were considered a factor in the transport of dust from Africa by Awad and Mashat (2014) or a factor in the transport of dust from the Syrian and Iraqi Deserts to the northern AP by Hamidi et al. (2013) and Notaro et al. (2013). Moreover, the pressure gradient lines were oriented more eastward than those in the WSC, and the distributions of atmospheric systems are similar to those of frontal dust systems (Hamidi et al., 2013; Prakash et al., 2015; Yu et al., 2015; Almazroui and Awad, 2016; Nabavi et al., 2016; Beegum et al., 2018; Hermida et al., 2018), Mediterranean storm tracks (Notaro et al., 2013;), and Saharan cyclone tracks (Hannachi et al., 2011); therefore, they are called frontal systems.

For the WRD composite, the most pronounced atmospheric system was the RST. In addition, the southern low pressure formed a pronounced trough over the western AP, with a wavy pressure gradient over the northern AP, in agreement with the results of Saaroni et al. (1998), Mashat and Awad (2015), Prakash et al. (2015), and Mashat et al. (2018). Other notable features included the pronounced Siberian ridge over the AG and the maximum wind core located over the eastern AP in a position farther north than that in the NRD composite. Therefore, this system is called the RST system.

The atmospheric dust systems in the ERD composite are characterized by a southern low-pressure system that forms wavy isobars and a pronounced trough over the eastern AP. The trough and core of the maximum wind are located over the eastern and southern AP, respectively, unlike in the other situations. Additionally, the southern low-pressure system deepens to 1 hPa, and the Azores high-pressure center is located farther north than in the WRD situation. This appears similar to the third shamal system described by Hamidi et al. (2013); additionally, it could be considered a thermal low system (Mohalfi et al., 1998; Johnson, 2003; Das et al., 2015; Jin and Sun, 2016) and therefore it is called the thermal low system.

At a pressure level of 850 hPa, most of the AP in the NRD, or the frontal system, was affected by the subtropical anticyclone, and the northern AP was affected by the trough of the northern cyclone. In the

WRD composite or the RST system, the subtropical anticyclone and northern cyclone retreated from the AP, while the tropical cyclone trough extended northward over the western AP. However, in the ERD composite or the thermal low system, the African branch of the subtropical anticyclone extended eastward to the western AP. The northern cyclone had a trough over the northern AP, and the cyclonic center over Iran formed a geopotential gradient area with the Arabian branch of the subtropical anticyclone over the AP and AG. This situation was explained by Hamidi et al. (2014) to be a factor responsible for emitting dust from local deserts or transporting dust from remote deserts. The interaction between the atmospheric systems oriented the geopotential gradient over the AG more in a north-south direction than in the other composites.

Although the features of the vertical velocity at 850 hPa are generally similar between the different dust composites, the highest values and their positions differ between the different composites. The centers of the core of the strongest vertical velocity (downward and upward) varied between the different dust situations. The cores were in the northern, central, and southern AP in the frontal system, the RST system, and the thermal low system, respectively. The distribution of the downward and upward motion forms two vertical cells, with the upward branch and two downward branches in the surrounding areas. Generally, the axis of the two vertical circles, with the axis passing between the downward-motion areas, rotated anticlockwise as the dust region shifted from the frontal system to the RST system and then to the thermal low system.

The atmospheric systems at 500 hPa indicated that the Middle East was influenced by the northern cyclone trough in the dust cases, but this trough shifted eastward and became less pronounced as the dust region shifted from the frontal system to the RST system and then to the thermal low system. In addition, the Arabian subtropical ridge became flat and shifted eastward as the dust region shifted anticlockwise from the frontal system to the RST system and then to the thermal low system. The wind speed at the 500-hPa level reached its highest value when the dust was affected by the thermal low system and reached its lowest value when the dust was affected by the RST system.

The relationship between the stability over the Mediterranean, Red Sea and AG plays an important role in the influence of dust storms on the area. This study shows that, when the stability over the Mediterranean decreased, dust storms influenced the northern region, but when the stability over the Mediterranean and AG increased, dust storms influenced the western region. Furthermore, dust storms influenced the eastern region when the stability increased over the Mediterranean and Red Sea regions. Additionally, the results indicated that the formation of dust events requires not only low stability (Alharbi et al., 2013) but also an interaction between regions of low and high stability.

The case study clearly differentiates among the synoptic features of the different regional dust patterns and confirms that low-pressure systems are the main systems associated with the frontal system, and the RST and its interactions with the Azores and Siberian ridges are the main synoptic features associated with the RST system. The deeper southern AP low-pressure system and its interaction with the Azores system and the high-pressure center over the northeastern AP are the main synoptic features associated with the thermal low system.

In addition, although the maximum wind forms a trough shape in all cases, the extended position of the core follows the dust region. The core is located over the eastern AP in the RST system, over the northern AP in the frontal system and over Africa and the northern AP in the thermal low system.

At the upper levels, the distribution of the atmospheric systems associated with dust storms in the different AP regions indicated that the northern cyclone trough enhanced the surface low pressure in the frontal system and that the extended tropical cyclone trough over the western region enhanced the RST at the surface in the RST system. However, the southern low pressure in the thermal low system was accompanied by a ridge between the trough over the AG and the trough over the central AP, enhancing the northwesterly wind over the eastern AP.

5. Conclusion

The spatial distribution of dust and dust storms over the AP demonstrated that most of the area north of 24º N is strongly affected by dust phenomena, as is

the Wadi-Aldawaser station, which is close to the desert. The temporal distribution demonstrated two periods for dust (dust storms), from 1978 to 1995 and from 1995 to 2008, with a high increasing rate and a low increasing (or decreasing) rate, respectively.

Synoptically, the spatial distribution of the atmospheric dust systems can be divided into three different systems with different characteristics, each mainly influencing the climate regions of the AP.

The northern system (or frontal system) consists of a surface low-pressure system, high-level troughs and a jet stream at the head of the troughs. This type of system forms an integrated system in which the maximum wind enhances the mid-level upward motion and increases the lifting force of the dust blown from local deserts, such as the Ad Dahna and the Syrian and Iraq deserts.

In the western system (or RST system), the RST and western trough of the southern low-pressure system were connected and deepened in the atmosphere via the northern extension of the upper tropical cyclone, and the trough-shaped maximum wind and upper-level trough were located over the western region (Shalaby et al., 2015; Mashat et al., 2019).

In the eastern system (or thermal low system), the southern low-pressure system formed a pronounced trough over the AG, accompanied by a subtropical anticyclonic center in the upper layers, which enhanced the thermal low (El Kenawy et al., 2014; El Kenawy and McCabe, 2016) or increased the surface temperature (Babu et al., 2016; Hasanean and Almazroui, 2016). Additionally, the pressure and geopotential gradients were oriented north-south, which might explain the formation of southerly shamal winds (Shao et al., 2011; Yu et al., 2016; Rashki et al., 2019) or high wind speeds (El-Sabh and Murty, 1989; Beegum et al., 2018; Hermida et al., 2018).

Widespread cases and previous studies (e.g., Goudi and Middleton, 2006; Hamidi et al., 2013; Mashat et al., 2018) have indicated that a combination of more than one of these systems could influence dust systems over the AP.

Generally, all cases are accompanied by pressure and geopotential gradients as factors involved in the generation of the wind responsible for emitting dust from the sources and transporting it to the affected regions (El-Sabh and Murty 1989; Hamidi et al., 2014, Beegum et al., 2018; Hermida et al., 2018). The shape and core of the maximum wind at 250 hPa follow the main atmospheric systems accompanying dust storm events in the different regions. The southern low-pressure system is the common atmospheric feature accompanying all dust systems. If this low pressure is located over Rub Al Khali or over another dominant dust area in the AP, local dust-source contributions are expected to influence the AP in all dust systems (Prospero et al., 2002; Giles, 2005; Notaro et al., 2013).

The atmospheric mechanisms influencing the dust and the expected dust sources in the Sahara, Syria, Iraq, and northern and eastern AP are considered. The dust systems over different regions can be classified into two mechanisms: dust-generating systems (frontal and thermal low systems) or dust-transporting systems (RST systems).

Acknowledgments

The authors are grateful to King Abdulaziz University for providing the facilities and logistical support for this study. The authors also acknowledge NASA and NCEP/NCAR for providing the meteorological data through their websites.

References

Abdi Vishkaee F, Flamant C, Cuesta J, Flamant P, Khalesifard H. 2011. Multi-platform observations of dust vertical distribution during transport over northwest Iran in the summertime. Journal of Geophysical Research 116: D05206. https://doi.org/10.1029/2010JD014573

Alharbi BH, Maghrabi A, Tapper N. 2013. The march 2009 dust event in Saudi Arabia: Precursor and supportive environment. Bulletin of the American Meteorological Society 94: 515-528. https://doi.org/10.1175/BAMS-D-11-00118.1

Alobaidi M, Almazroui M, Mashat A, Jones PD. 2017. Arabian Peninsula wet season dust storm distribution: Regionalization and trends analysis (1983-2013). International Journal of Climatology 37: 1356-1373. https://doi.org/10.1002/joc.4782

Ali MA, Assiri M, Dambul R. 2017. Seasonal aerosol optical depth (AOD) variability using satellite data and its comparison over Saudi Arabia for the period 2002-2013. Aerosol and Air Quality Research 17, 1267-1280. https://doi.org/10.4209/aaqr.2016.11.0492

Al-Jumaily KJ, Ibrahim MK. 2013. Analysis of synoptic situation of dust storms in Iraq. International Journal of Energy and Environment 4: 851-858. https://doi.org/10.14456/ea.2021.2

Almazroui M, Awad AM. 2016. Synoptic regimes associated with the eastern Mediterranean wet season cyclone tracks. Atmospheric Research 180: 92-118. https://doi.org/10.1016/j.atmosres.2016.05.015

Al-Yahyai S, Charabi Y. 2014. Trajectory calculation as forecasting support tool for dust storms. Advances in Meteorology 2014: 698359. https://doi.org/10.1155/2014/698359

Archer D, Winguth A, Lea D, Mahowald N. 2000. What caused the glacial/interglacial atmospheric pCO_2 cycles? Reviews of Geophysics 38 (2): 159-189. https://doi.org/10.1029/1999RG000066LMartin

Awad AM, Mashat AS. 2014. Synoptic features associated with dust transition processes from North Africa to Asia. Arabian Journal of Geosciences 7: 2451-2467. https://doi.org/10.1007/s12517-013-0923-4

Awad AM, Mashat AS. 2016. Synoptic characteristics of spring dust days over northern Saudi Arabia. Air Quality, Atmosphere & Health 9: 41-50. https://doi.org/10.1007/s11869-015-0320-0

Babu CA, Jayakrishnan PR, Varikoden H. 2016. Characteristics of precipitation pattern in the Arabian Peninsula and its variability associated with ENSO. Arabian Journal of Geosciences 9: 186. https://doi.org/10.1007/s12517-015-2265-x

Beegum SN, Gherboudj I, Chaouch N, Temimi M, Ghedira H. 2018. Simulation and analysis of synoptic scale dust storms over the Arabian Peninsula. Atmospheric Research 199: 62-81. https://doi.org/10.1016/j.atmosres.2017.09.003

Butt MJ, Assiri ME, Ali MA. 2017. Assessment of AOD variability over Saudi Arabia using MODIS Deep Blue products. Environmental Pollution 231: 143-153. https://doi.org/10.1016/j.envpol.2017.07.104

Das S, Dey S, Dash SK, Giuliani G, Solmon F. 2015. Dust aerosol feedback on the Indian summer monsoon: Sensitivity to absorption property. Journal of Geophysical Research: Atmospheres 120 (18): 9642-9652. https://doi.org/10.1002/2015JD023589

Dentener FJ, Carmichael GR, Zhang Y, Lelieveld J, Crutzen PJ. 1996. Role of mineral dust aerosol as a reactive surface in the global troposphere. Journal of Geophysical Research: Atmospheres 101 (D17): 22869-22889. https://doi.org/10.1029/96JD01818

Dickerson RR, Kondragunta S, Stenchikov G, Civerolo KL, Doddridge BG, Holben B. 1997. The impact of aerosols on solar UV radiation and photochemical smog. Science 278: 827-830. https://doi.org/10.1126/science.278.5339.827

El Kenawy AM, McCabe MF, Stenchikov G, Raj J. 2014. Multi-decadal classification of synoptic weather types, observed trends and links to rainfall characteristics over Saudi Arabia. Frontiers in Environmental Science 2: 37. https://doi.org/10.3389/fenvs.2014.00037

El Kenawy AM, McCabe MF. 2016. A multi-decadal assessment of the performance of gauge- and model-based rainfall products over Saudi Arabia: Climatology, anomalies and trends. International Journal of Climatology 36: 656. https://doi.org/10.1002/joc.4374

El-Sabh MI, Murty TS. 1989. Storm surges in the Arabian Gulf. Natural Hazards 1: 371-385. https://doi.org/10.1007/BF00134834

Francis D, Alshamsi N, Cuesta J, Isik AG, Dundar C. 2019. Cyclogenesis and density currents in the Middle East and the associated dust activity in September 2015. Geosciences 9: 376. https://doi.org/10.3390/geosciences9090376

Francis D, Chaboureau JP, Nelli N, Cuesta J, Al Shamsi N, Temimi M, Pauluis O, Xue L. 2020. Summertime dust storms over the Arabian Peninsula and impacts on radiation, circulation, cloud development and rain. Atmospheric Research 250: 105364. https://doi.org/10.1016/j.atmosres.2020.105364

Gandham H, Dasari HP, Langodan S, Karumuri RK, Hoteit I. 2020. Major changes in extreme dust events dynamics over the Arabian Peninsula during 2003-2017 driven by atmospheric conditions. Journal of Geophysical Research: Atmospheres 125: 1-20. https://doi.org/10.1029/2020JD032931

Gates WL. 1961. Static stability measures in the atmosphere. J Meteor 18, 526-533. https://doi.org/10.1175/1520-0469(1961)018<0526:SSMITA>2.0.CO;2

Giles J. 2005. Climate science: The dustiest place on Earth. Nature 434, 816-819. https://doi.org/10.1038/434816a

Goudie AS, Middleton NJ. 2001. Saharan dust storms: Nature and consequences. Earth-Science Reviews 56: 179-204. https://doi.org/10.1016/S0012-8252(01)00067-8

Goudie AS, Middleton NJ. 2006. Desert dust in the global system. Springer Science & Business Media, Heidelberg, 288 pp. https://doi.org/10.1007/3-540-32355-4

Goudie AS, Goudie AM, Viles HA. 2021. The distribution and nature of star dunes: A global analysis. Aeolian

Researchearch 50, 100685. https://doi.org/10.1016/j.aeolia.2021.100685

Hamidi M, Kavianpour MR, Shao Y. 2013. Synoptic analysis of dust storms in the Middle East. Asia-Pacific Journal of Atmospheric Sciences 49: 279-286. https://doi.org/10.1007/s13143-013-0027-9

Hamidi M, Kavianpour MR, Shao Y. 2014. Numerical simulation of dust events in the Middle East. Aeolian Researchearch 37: 59-70. https://doi.org/10.1016/j.aeolia.2014.02.002

Hamidi M, Kavianpour MR, Shao Y. 2017. A quantitative evaluation of the 3-8 July 2009 Shamal dust storm. Aeolian Research 24: 133-143. https://doi.org/10.1016/j.aeolia.2016.12.004

Hamidi M. 2019. Atmospheric investigation of frontal dust storms in Southwest Asia. Asia-Pacific Journal of Atmospheric Sciences 55: 177-193. https://doi.org/10.1007/s13143-018-0083-2

Hamzeh NH, Karami S, Kaskaoutis DG, Tegen I, Moradi M, Opp C. 2021. Atmospheric dynamics and numerical simulations of six frontal dust storms in the Middle East region. Atmosphere 12: 125. https://doi.org/10.3390/atmos12010125

Hannachi A, Awad A, Ammar K. 2011. Climatology and classification of spring Saharan cyclone tracks. Climate Dynamics 37: 473-491. https://doi.org/10.1007/s00382-010-0941-9

Hasanean HM, Almazroui M. 2016. Teleconnections of the tropical sea surface temperatures to the surface air temperature over Saudi Arabia in summer season. International Journal of Climatology 37: 1040-1049. https://doi.org/10.1002/joc.4758

Hermida L, Merino A, Sánchez JL, Fernández-González S, García-Ortega E, López L. 2018. Characterization of synoptic patterns causing dust outbreaks that affect the Arabian Peninsula. Atmospheric Research 199: 29-39. https://doi.org/10.1016/j.atmosres.2017.09.004

Houssos EE, Chronis T, Fotiadi A, Hossain F. 2015. Atmospheric circulation characteristics favoring dust outbreaks over the Solar Village, central Saudi Arabia. Monthly Weather Review 143: 3263-3275. https://doi.org/10.1175/MWR-D-14-00198.1

Islam MN, Almazroui M. 2012. Direct effects and feedback of desert dust on the climate of the Arabian Peninsula during the wet season: A regional climate model study. Climate Dynamics 39: 2239-2250. https://doi.org/10.1007/s00382-012-1293-4

Jish Prakash P, Stenchikov G, Kalenderski S, Osipov S, Bangalath H. 2015. The impact of dust storms on the Arabian Peninsula and the Red Sea. Atmospheric Chemistry and Physics 15: 199-222. https://doi.org/10.5194/acp-15-199-2015

Jin Z, Sun M. 2016. An initial study on climate change fingerprinting using the reflected solar spectra. Journal of Climate 29: 2781-2796. https://doi.org/10.1175/JCLI-D-15-0297.1

Johnson RH. 2003. Thermal low. In: Encyclopedia of atmospheric science (Holton J, Pyle J, Curry JA, Eds.). Academic Press, London, United Kingdom, 2269-2273.

Kalenderski S, Stenchikov G, Zhao C. 2013. Modeling a typical winter-time dust event over the Arabian Peninsula and the Red Sea. Atmospheric Chemistry and Physics 13: 1999-2014. https://doi.org/10.5194/acp-13-1999-2013

Kalnay E, Kanamitsu M, Kistler R, Collins W, Deaven D, Gandin L, Iridell M, Saha S, White G, Woollen J, Zhu Y, Chelliah M, Ebisuzaki W, Higgins W, Janowiak J, Mo KC, Ropolewski C, Wang J, Leetma A, Reynolds R, Jenne R, Joseph D. 1996. The NCEP/NCAR 40-year reanalysis project. Bulletin of the American Meteorological Society 77: 437-471. https://doi.org/10.1175/1520-0477(1996)077<0437:TNYRP>2.0.CO;2

Kaskaoutis DG, Francis D, Rashki A, Chaboureau JP, Dumka UC. 2019. Atmospheric dynamics from synoptic to local scale during an intense frontal dust storm over the Sistan Basin in winter 2019. Geosciences 2019: 453. https://doi.org/10.3390/geosciences9100453

Kistler R, Collins W, Saha S, White G, Woollen J, Kalnay E, Chelliah M, Ebisuzaki W, Kanamitsu M, Kousky V, van den Dool H, Jenne R, Fiorino M. 2001. The NCEP/NCAR 50-year reanalyses: Monthly CD-ROM and documentation. Bulletin of the American Meteorological Society 82: 247-267. https://doi.org/10.1175/1520-0477(2001)082<0247:TNNYRM>2.3.CO;2

Kok JF, Ward DS, Mahowald NM, Evan AT. 2018. Global and regional importance of the direct dust-climate feedback. Nature Communications 9: 241. https://doi.org/10.1038/s41467-017-02620-y

Kutiel H, Furman H. 2003. Dust storms in the middle east: Sources of origin and their temporal characteristics. Indoor and Built Environment 12: 419-426. https://doi.org/10.1177/1420326X03037110

Liu Y, Jia R, Dai T, Xie Y, Shi G. 2014. A review of aerosol optical properties and radiative effects. Journal of Meteorological Research 28: 1003-1028. https://doi.org/10.1007/s13351-014-4045-z

Martin JH. 1991. Iron still comes from above. Nature 353: 123. https://doi.org/10.1038/353123b0

Martin RV, Jacob DJ, Yantosca RM, Chin M, Ginoux P. 2003. Global and regional decreases in tropospheric oxidants from photochemical effects of aerosols. Journal of Geophysical Research 108 (D3): 4097. https://doi.org/10.1029/2002JD002622

Mashat AS, Awad AM. 2016. Synoptic characteristics of the primary widespread winter dust patterns over the northern Arabian Peninsula. Air Quality, Atmosphere & Health 9: 503-516. https://doi.org/10.1007/s11869-015-0357-0

Mashat AS, Alamoudi AO, Awad AM, Assir ME. 2017. Synoptic characteristics of dusty spring days over central and eastern Saudi Arabia. Air Quality, Atmosphere & Health 10: 307. https://doi.org/10.1007/s11869-016-0420-5

Mashat AS, Alamoudi AO, Awad AM, Assiri ME. 2018. Seasonal variability and synoptic characteristics of dust cases over southwestern Saudi Arabia. International Journal of Climatology 38: 105-124. https://doi.org/10.1002/joc.5164

Mashat AS, Alamoudi AO, Awad AM, Assiri ME, 2019. Monthly and seasonal variability of dust events over northern Saudi Arabia. International Journal of Climatology 40: 1607-1629. https://doi.org/10.1002/joc.6290

Mashat AS, Awad AM, Assiri ME, Labban AH. 2021. Synoptic pattern of the Red Sea trough associated with spring dust over the northern and western Arabian Peninsula. Meteorology and Atmospheric Physics 133: 655-673. https://doi.org/10.1007/s00703-020-00771-0

Middleton N. 1986. A geography of dust storms in Southwest Asia. Journal of Climatology 6: 183-196. https://doi.org/10.1002/joc.3370060207

Middleton N. 2019. Variability and trends in dust storm frequency on decadal timescales: Climatic drivers and human impacts. Geosciences 9: 261. https://doi.org/10.3390/geosciences9060261

Mohalfi S, Bedi HS, Krishnamurti TN, Cocke SD. 1998. Impact of shortwave radiative effects of dust aerosols on the summer season heat low over Saudi Arabia. Monthly Weather Review 126: 3153-3168. https://doi.org/10.1175/1520-0493(1998)126<3153:IOSREO>2.0.CO;2

Mohammadpour K, Sciortino M, Kaskaoutis DG. 2021. Classification of weather clusters over the Middle East associated with high atmospheric dust-AODs in west Iran. Atmospheric Research 259: 105682. https://doi.org/10.1016/j.atmosres.2021.105682

Mohammadpour K, Rashki A, Sciortino M, Kaskaoutis D, Darvishi BA. 2022. A statistical approach for identification of dust-AOD hotspots climatology and clustering of dust regimes over Southwest Asia and the Arabian Sea. Atmospheric Pollution Research 13: 101395. https://doi.org/10.1016/j.apr.2022.101395

Nabavi SO, Haimberger L, Samimi C. 2016. Climatology of dust distribution over West Asia from homogenized remote sensing data. Aeolian Research 21, 93-107. https://doi.org/10.1016/j.aeolia.2016.04.002

Nabavi SO, Haimberger L, Samimi C. 2017. Sensitivity of WRF-chem predictions to dust source function specification in West Asia. Aeolian Research 24: 115-131. https://doi.org/10.1016/j.aeolia.2016.12.005

Namdari S, Karimi N, Sorooshian A, Mohammadi G, Sehatkashani S. 2018. Impacts of climate and synoptic fluctuations on dust storm activity over the Middle East. Atmospheric Environment 173: 265-276. https://doi.org/10.1016/j.atmosenv.2017.11.016

Notaro M, Alkolibi F, Fadda E, Bakhrjy F. 2013. Trajectory analysis of Saudi Arabian dust storms. Journal of Geophysical Research: Atmospheres 118: 6028-6043. https://doi.org/10.1002/jgrd.50346

Notaro M, Yu Y, Kalashnikova OV. 2015. Regime shift in Arabian dust activity, triggered by persistent fertile crescent drought. Journal of Geophysical Research: Atmospheres 120: 10229-10249. https://doi.org/10.1002/2015JD023855

Osetinsky I, Alpert P. 2006. Calendaricities and multimodality in the Eastern Mediterranean cyclonic activity. Natural Hazards and Earth System Sciences 6: 587-596. https://doi.org/10.5194/nhess-6-587-2006

Prakash PJ, Stenchikov G, Kalenderski S, Osipov S, Bangalath H. 2015. The impact of dust storms on the Arabian Peninsula and the Red Sea. Atmospheric Chemistry and Physics 15: 199-222. https://doi.org/10.5194/acp-15-199-2015

Perrone TJ. 1981. Winter Shamal in the Persian Gulf. Technical Report IR 79-06. 2nd ed. Naval Environmental Prediction Research Facility, Monterey, Ca.

Prospero J. 1999. Long-term measurements of the transport of African mineral dust to the southeastern United States: Implications for regional air quality. Journal of

Geophysical Research 104: 15917-15927. https://doi.org/10.1029/1999JD900072

Prospero JM, Ginoux P, Torres O, Nicholson SE, Gill TE. 2002. Environmental characterization of global sources of atmospheric soil dust identified with the Nimbus 7 total ozone mapping spectrometer (TOMS) absorbing aerosol product. Reviews of Geophysics 40: 2-1-2-31. https://doi.org/10.1029/2000RG000095

Rao PG, Al-Sulaiti M, Al-Mulla AH. 2001. Winter Shamals in Qatar, Arabian Gulf. Weather 56: 444-451. https://doi.org/10.1002/j.1477-8696.2001.tb06528.x

Rashki A, Arjmand M, Kaskaoutis D. 2017. Assessment of dust activity and dust-plume pathways over Jazmurian Basin, southeast Iran. Aeolian Research 24: 145-160. https://doi.org/10.1016/j.aeolia.2017.01.002

Rashki A, Kaskaoutis DG, Mofidic A, Minvielled F, Chiapellod I, Legrandd M, Dumkae UC. 2019. Effects of Monsoon, Shamal and Levar winds on dust accumulation over the Arabian Sea during summer – The July 2016 case. Aeolian Research 36: 27-44. https://doi.org/10.1016/j.aeolia.2018.11.002

Rezazadeh M, Irannejad P, Shao Y. 2013. Climatology of the Middle East dust events. Aeolian Research 10: 103-109. https://doi.org/10.1016/j.aeolia.2013.04.001

Saaroni H, Ziv B, Bitan A, Alpert P. 1998. Easterly wind storms over Israel. Theoretical and Applied Climatology 59: 61-77. https://doi.org/10.1007/s007040050013

Shalaby A, Rappenglueck B, and Eltahir EAB. 2015. The climatology of dust aerosol over the arabian peninsula. Atmospheric Chemistry and Physics Discussions 15: 1523-1571. https://doi.org/10.5194/acpd-15-1523-2015

Shao Y, Wyrwoll KH, Chappell A, Huang J, Lin Z, McTainsh GH, Yoon S. 2011. Dust cycle: An emerging core theme in Earth system science. Aeolian Research 2: 181-204. https://doi.org/10.1016/j.aeolia.2011.02.001

Sissakian VK, Al-Ansari N, Knutsson S. 2013. Sand and dust storm events in Iraq. Journal of Natural Science 5: 1084-1094. https://doi.org/10.4236/ns.2013.510133

Tanaka TY, Chiba M. 2006. A numerical study of the contributions of dust source regions to the global dust budget. Global Planetary Changes 52: 88-104. https://doi.org/10.1016/j.gloplacha.2006.02.002

Washington R, Todd M, Middleton NJ, Goudie AS. 2003. Dust-storm source areas determined by the total ozone monitoring spectrometer and surface observations. Annals of the Association of American Geographers 93: 297-313. https://doi.org/10.1111/1467-8306.9302003

Washington R, Todd MC. 2005. Atmospheric controls on mineral dust emission from the Bodélé Depression, Chad: The role of the low-level jet. Geophysical Research Letters 32: L17701. https://doi.org/10.1029/2005GL023597

WMO. 2005. Climate and land degradation. World Meteorological Organization, Geneva, Switzerland.

Yassin M, Almutairi S, Al-Hemoud A. 2018. Dust storms backward trajectories and source identification over Kuwait. Atmospheric Research 212: 158-171. https://doi.org/10.1016/j.atmosres.2018.05.020

Yu Y, Notaro M, Liu Z, Kalashnikova O, Alkolibi F, Fadda E, Bakhrjy F. 2013. Assessing temporal and spatial variations in atmospheric dust over Saudi Arabia through satellite, radiometric, and station data. Journal of Geophysical Research: Atmospheres 118: 13253-13264. https://doi.org/10.1002/2013JD020677

Yu Y, Notaro M, Liu Z, Wang F, Alkolibi F, Fadda E, Bakhrjy F. 2015. Climatic controls on the interannual to decadal variability in Saudi Arabian dust activity: Toward the development of a seasonal dust prediction model. Journal of Geophysical Research: Atmospheres 120: 1739-1758. https://doi.org/10.1002/2014JD022611

Yu Y, Notaro M, Kalashnikova OV, Garay MJ. 2016. Climatology of summer Shamal wind in the Middle East. Journal of Geophysical Research: Atmospheres 121: 289-305. https://doi.org/10.1002/2015JD024063

Zhao S, Zhang H, Feng S, Fu Q. 2015. Simulating direct effects of dust aerosol on arid and semi-arid regions using an aerosol-climate coupled system. International Journal of Climatology 35: 1858-1866. https://doi.org/10.1002/joc.4093

Zoljoodi M, Didevarasl A, Saadatabadi AR. 2013. Dust events in the western parts of Iran and the relationship with drought expansion over the dust-source areas in Iraq and Syria. Atmospheric and Climate Sciences 3: 321-336. https://doi.org/10.4236/acs.2013.33034

Supplementary Material

Table S1. Detailed information on the stations used in Figure 1b.

ID	Station	WMO code	Latitude	Longitude	Elevation (m)
1	Turaif	403560	31.68	38.73	852
2	Guriat	403600	31.40	37.28	504
3	Arar	403570	30.9	41.1	550
4	Aljouf	403610	29.78	40.1	670
5	Tabuk	403750	28.38	36.6	770
6	Hail	403940	27.43	41.7	1000
7	Alwejh	404000	26.2	36.5	20
8	Rafha	403620	29.61	43.5	445
9	Alqaisumah	403730	28.32	46.1	360
10	Hafrbaten	403770	27.90	45.53	413
11	Riyadh Old	404380	24.71	46.73	610
12	Riyadh new	404370	24.93	46.7	612
13	Dhahran	404160	26.26	50.16	22
14	Alhasa	404200	25.4	49.5	180
15	Gassim	404050	26.	3 43.8	648
16	Almadinah	404300	24.55	39.7	630
17	Yenbo	404390	24.13	38.1	8
18	Jeddah	410240	21.7	39.2	18
19	Makkah	410300	21.43	39.8	273
20	Altaif	410360	21.48	40.6	1455
21	Albaha	410550	20.3	41.7	1655
22	Wadi Aldawaser	410620/610	20.5	45.3	615
23	Bisha	410840	19.98	42.6	1167
24	Khamis Mushait	411140	18.3	42.8	2047
25	Abha	411120	18.23	42.7	2100
26	Najran	411280	17.61	44.4	1213
27	Gizan	411400	16.88	42.6	4

S1. Climate synoptic characteristics of the classified regions

S1.1 Geopotential height at 500 hPa and the static stability layer from 1000 to 500 hPa

The northern cyclone in the composite of the cases affecting the NRD, with a value of 5540 gpm (Fig. S1a), has a trough over the eastern Mediterranean and Egypt, i.e., to the west of that in the WSC. The subtropical anticyclone, with a value of 5880 gpm, has two ridges: one over Africa and the western Mediterranean and the other over the AP and Iran. These two atmospheric systems form an area of geopotential gradient over Egypt, the eastern Mediterranean, the AP and the Levant. The wind in this composite reaches its maximum value over the northern AP and weakens to the north and southward.

A belt of low stability (Fig. S1a) is observed over the Sahara, the AP and Iran, with values of 0.5 deg db^{-1} over the Sahara and 0.4 deg db^{-1} over the AP and Iran. The low-stability belt is surrounded to the north and south by belts of high stability, with maximum values of 1.1 and 0.9 deg db^{-1} over the Arabian Sea and the Mediterranean, respectively. In addition, relatively high stability is observed over the Red Sea and AG, with values of 0.65 and 0.55 deg db^{-1}, respectively. These regions with different stabilities form a stability gradient area around the AP.

The composite of dust events in the WRD (Fig. S1b) shows that the trough of the northern cyclone, with a value of 5540 gpm, is oriented more eastward and appears relatively flatter than those in the NRD and WSC. Additionally, the gradient in geopotential over the eastern Mediterranean, AP, and Levant is lower. The wind speed is lower over the northern AP but increases southward.

For dust in the WRD (Fig. S1b), the stability over Africa decreased with respect to that in the NRD to 0.4 deg db^{-1}, and the stability over the eastern

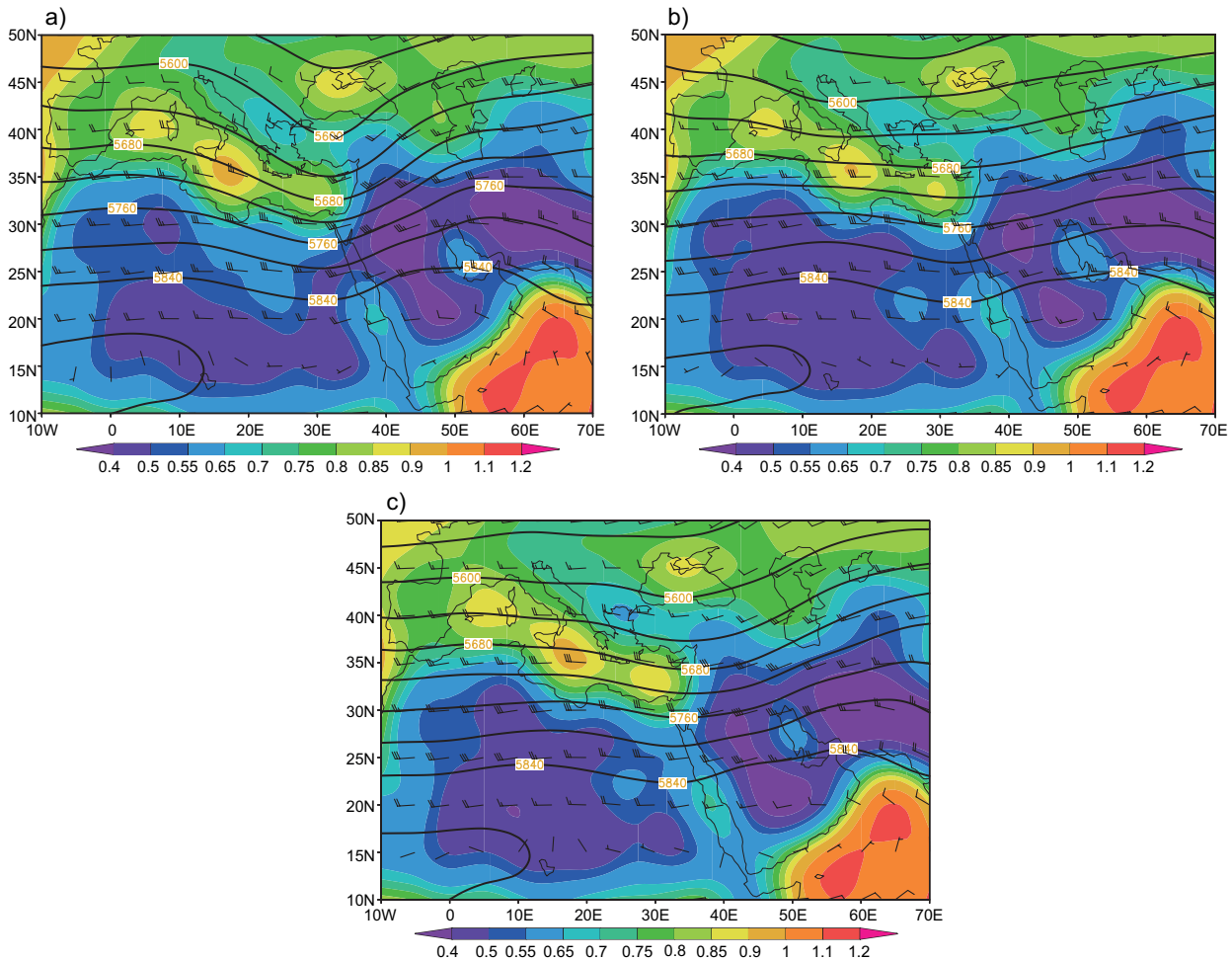

Fig. S1. Geopotential height distributions and wind vectors at the 500-hPa pressure level and static stability in the layer between 1000 hPa and 500 hPa (contours in gpm, barbs in knots and shading in deg db^{-1}, respectively) for regional composites of the (a) northern (b) western, and (c) eastern regions.

Mediterranean and AG increased to 0.85 and 0.6 deg db^{-1}, respectively. Additionally, the areas of low stability over the northern and southern AP shrank and expanded, respectively.

Based on the composite of dust events in the ERD (Fig. S1c), the trough of the northern cyclone shifted eastward compared with that in the above composites. Additionally, a new weak trough appeared over the eastern AP. The wind in this composite is higher than that in the NRD composite but decreases rapidly northward.

Although the general features of the stability distribution for dust in the ERD (Fig. S1c) are similar to those in the composite for the other regions, the stability increased over the Red Sea to 0.7 deg db^{-1} and decreased over the AG to 0.55 deg db^{-1}. Additionally, the low-stability area over the northern AP shrank.

S2. Case study

S2.1 Geopotential height at 500 hPa and the static stability layer at 1000-500 hPa

The northern cyclone associated with the NRD cases (Fig. S2a), with a value of 5540 gpm, has a deep trough over the eastern Mediterranean and eastern Africa. The subtropical anticyclone, with a value of 5880 gpm, has pronounced ridges over western Africa and the AP. The wind over the AP and Levant decreases from west to east and from north to south.

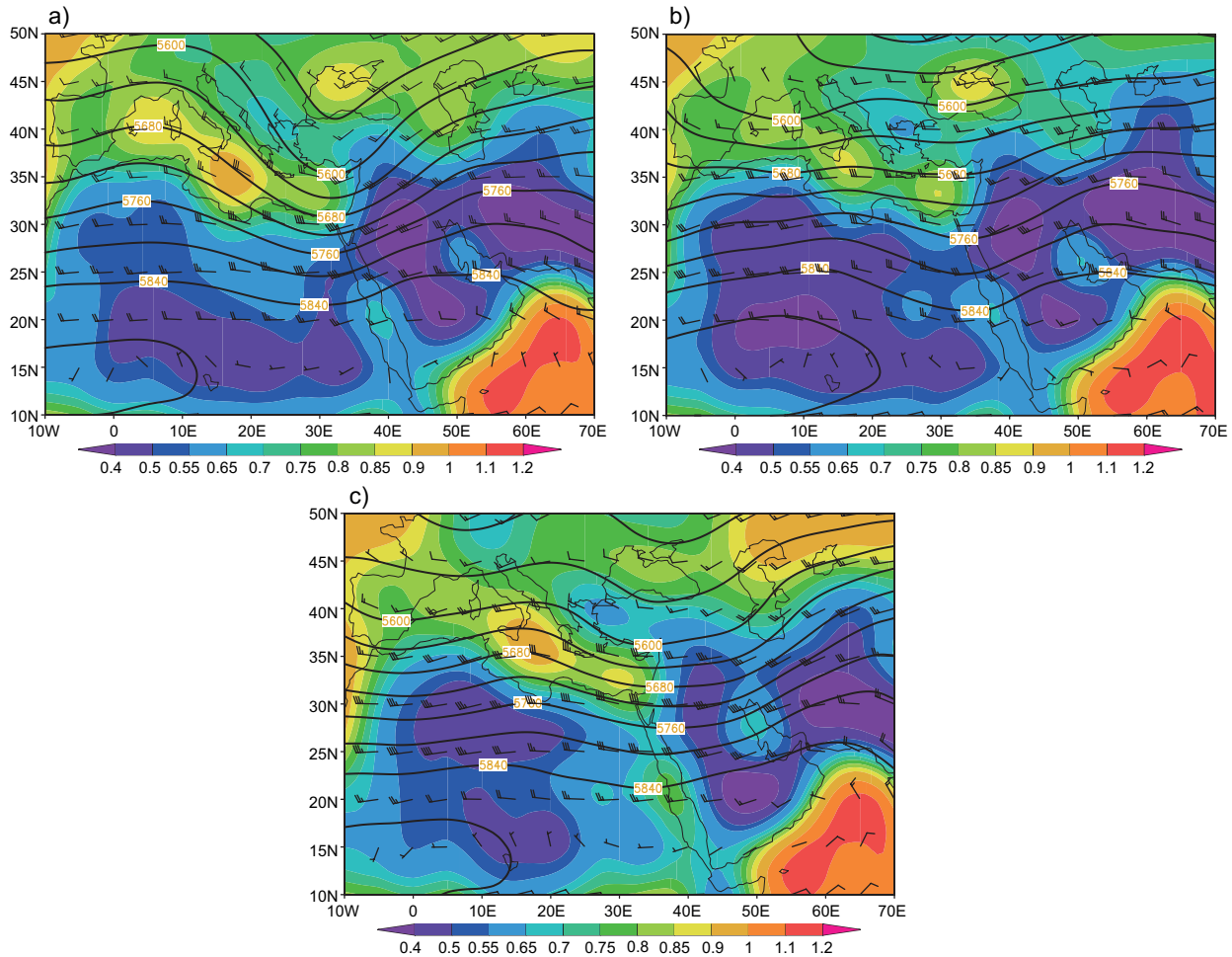

Fig. S2. Geopotential height distributions and wind vectors at the 500-hPa pressure level and static stability in the layer between 1000 hPa and 500 hPa (contours in gpm, barbs in knots and shading in deg db^{-1}, respectively) for regional composites of the (a) northern (b) western, and (c) eastern regions.

The stability distribution for the NRD cases (Fig. S2a) shows that the low stability over the AP, Iran and Pakistan has a value of 0.4 deg db^{-1}, while that over southern Africa has a value of 0.5 deg db^{-1}. The low stability over the AP is surrounded by high-stability areas with values of 1.1 deg db^{-1} over the Arabian Sea, 1.0 deg db^{-1} over the Mediterranean, 0.65 deg db^{-1} over the Red Sea, and 0.55 deg db^{-1} over AG. The interaction of low-stability areas over the AP with the surrounding high-stability areas forms areas with stability gradients around the AP.

For the WRD cases (Fig. S2b), the trough of the northern cyclone, with a value of 5520 gpm, is shifted eastward compared with that of the NRD cases. In addition, the ridge of the subtropical anticyclone, with a value of 5880 gpm, is shifted eastward and is relatively flatter. The wind speed has the highest value over the central AP and decreases eastward, and generally the wind speed decreases southward from the northern AP.

For the WRD cases (Fig. S2b), the eastern Mediterranean stability increased to 0.85 deg db^{-1} compared with that of the NRD cases, while the stability over Africa decreased to 0.4 deg db^{-1}. In addition, the stability over the Red Sea shrank, while the stability over the AG increased and expanded. In general, this distribution of stability formed two centers of

low stability, with values of 0.4 deg db^{-1}, over the northern and southern AP.

For the ERD cases (Fig. S2c), the trough of the northern cyclone, with a value of 5520 gpm, is shifted eastward compared with that of the WRD cases. The Arabian ridge is flat, while the African ridge becomes pronounced. The wind speed increases more in this composite than in the other composites, although it decreases from west to east and from north to south.

The stability distribution of the ERD cases (Fig. S2c) shows that the low-stability area over the AP is located over the southern region and has a value of 0.4 deg db^{-1}. However, the high-stability areas over the Mediterranean and Red Sea are larger than in other composites, with values of 0.85 and 0.75 deg db^{-1}, respectively, and the stability over the AG expanded.